Heat stress intensification in the Mediterranean climate change hotspot

Noah S. Diffenbaugh,[1] Jeremy S. Pal,[2,3] Filippo Giorgi,[2] and Xuejie Gao[2,4]

Received 13 March 2007; accepted 14 May 2007; published 15 June 2007.

[1] We find that elevated greenhouse gas concentrations dramatically increase heat stress risk in the Mediterranean region, with the occurrence of hot extremes increasing by 200 to 500% throughout the region. This heat stress intensification is due to preferential warming of the hot tail of the daily temperature distribution, with 95th percentile maximum and minimum temperature magnitude increasing more than 75th percentile magnitude. This preferential warming of the hot tail is dictated in large part by a surface moisture feedback, with areas of greatest warm-season drying showing the greatest increases in hot temperature extremes. Fine-scale topographic and humidity effects help to further dictate the spatial variability of the heat stress response, with increases in dangerous Heat Index magnified in coastal areas. Further, emissions deceleration substantially mitigates heat stress intensification throughout the Mediterranean region, implying that emissions reductions could reduce the risk of increased heat stress in the coming decades. **Citation:** Diffenbaugh, N. S., J. S. Pal, F. Giorgi, and X. Gao (2007), Heat stress intensification in the Mediterranean climate change hotspot, *Geophys. Res. Lett.*, *34*, L11706, doi:10.1029/2007GL030000.

1. Introduction

[2] Global greenhouse gas (GHG) concentrations have steadily increased since the beginning of the industrial era [*Intergovernmental Panel on Climate Change* (*IPCC*), 2001]. Instrumental records reveal prolonged warming not only at Earth's surface [*IPCC*, 2001], but also in the troposphere [e.g., *Mears and Wentz*, 2005] and oceans [*Barnett et al.*, 2005]. Continued emissions of GHGs are likely to result in further global warming of approximately 2 to 6°C by the end of this century [*IPCC*, 2001], with changes in climate extremes likely to have substantially greater impact than changes in climate means [e.g., *White et al.*, 2006].

[3] Extreme heat exerts particular tolls on human systems, impacting human health [e.g., *Poumadere et al.*, 2005], energy supply and demand [e.g., *Smoyer-Tomic et al.*, 2003], and hydrological [*Tereshchenko et al.*, 2002] and agricultural resources [*Ferris et al.*, 1998]. In Europe, the summer of 2003 was the hottest of the past 500 years [*Luterbacher et al.*, 2004; *Schar et al.*, 2004], with mean temperatures exceeding the late-20th century baseline by up to 5 standard deviations [*Schar et al.*, 2004]. Excess deaths totaled 15,000 in France alone [*Poumadere et al.*, 2005], primarily associated with an extended period of extremely high maximum and minimum daily temperatures [*Poumadere et al.*, 2005].

[4] Here we explore the potential for GHG-induced changes in heat stress in the Mediterranean region. The Mediterranean region has been identified as one of the climate system's most responsive hotspots in the face of increased GHG forcing, particularly because of pronounced mean warming, large decreases in precipitation, and increases in inter-annual warm-season variability [*Giorgi*, 2006]. The sensitivity of the region, coupled with existing vulnerabilities to severe heat, provide motivation for understanding the mechanisms by which heat stress could respond to elevated GHG concentrations. However, although increasing GHG concentrations are likely to make hot summers more common in the coming decades [*Schar et al.*, 2004], a number of important uncertainties remain. For instance, whether changes in daily-scale temperature extremes will be dictated by uniform or non-uniform warming of the daily temperature distribution remains a key question [*Sanchez et al.*, 2004]. Additionally, the physiography of the Mediterranean region is extremely complex, and it is not known how fine-scale climate processes associated with topography, coastal interfaces, and land cover heterogeneity will regulate the magnitude and spatial variability of the heat stress response. Further, a broad range of potential global emissions pathways are still possible [*IPCC*, 2000], and differences in the response of heat stress to high and low emissions scenarios have not yet been quantified.

2. Methods

[5] We analyze the simulations described by *Gao et al.* [2006], which use the Abdus Salam ICTP regional climate model RegCM3 [*Pal et al.*, 2007]. In these simulations, RegCM3 is run on a 20 km resolution grid covering the Mediterranean region. Lateral boundary conditions are provided by 50 km resolution simulations driven by the HadAM3H atmospheric general circulation model (GCM) [*Giorgi et al.*, 2004a, 2004b]. In this "double-nested" mode, a higher resolution limited area grid is nested within a lower resolution limited area grid, much as a single limited area grid is nested within a global GCM or reanalysis grid. Output from the outer nested grid (50 km horizontal resolution with 14 sigma levels in the vertical) is interpolated to higher resolution and used as lateral boundary conditions for the inner nested grid (20 km horizontal resolution with 18 sigma levels in the vertical). In order to maintain consistency between the nested simulations, the

[1] Purdue Climate Change Research Center and Department of Earth and Atmospheric Sciences, Purdue University, West Lafayette, Indiana, USA.
[2] Abdus Salam International Centre for Theoretical Physics, Trieste, Italy.
[3] Now at Frank R. Seaver College of Science and Engineering, Loyola Marymount University, Los Angeles, California, USA.
[4] Now at National Climate Center, Beijing, China.

0094-8276/07/2007GL030000$05.00

physics options are the same between our outer (50 km) and inner (20 km) grids [*Gao et al.*, 2006].

[6] Our experimental strategy follows that of the PRUDENCE project [*Christensen et al.*, 2002]. We analyze three simulations: MED20RF, MED20B2 and MED20A2. MED20RF covers the period 1961–1989. MED20B2 and MED20A2 cover the period 2071–2099 under the IPCC SRES B2 and A2 emissions scenarios [*IPCC*, 2000], respectively. These two scenarios represent two distinct global GHG emissions pathways, with atmospheric carbon dioxide concentrations exceeding 600 ppmv (B2) and 800 ppmv (A2) by the end of the 21st century. The A2 scenario is thus a high-end emissions scenario in which global population growth is high and "global environmental concerns are relatively weak" [*IPCC*, 2000], while the B2 scenario lies close to the low end of the IPCC range, with slower population growth and "increased concern for environmental and social sustainability" relative to the A2 scenario [*IPCC*, 2000]. We define the deceleration effect as the reduction in heat stress intensification in the B2 scenario relative to the A2 scenario (MED20B2 minus MED20A2).

[7] Sea surface temperatures (SSTs) for the RF simulations are provided by the HadISST observed dataset [*Rayner et al.*, 2003]. SSTs for the B2 and A2 simulations are calculated by the HadCM3 coupled atmosphere-ocean GCM, the ocean component of which is configured at 1.25° × 1.25° resolution [*Johns et al.*, 2003]. B2 and A2 SSTs are prescribed in HadAM3H and RegCM3 after adding the HadCM3-calculated "perturbation" to the HadISST dataset as described by *Giorgi et al.* [2004b]. The A2 and B2 Mediterranean SSTs thus reflect the ability of the HadCM3 coupled model to accurately capture the Mediterranean ocean dynamics at 1.25° resolution.

[8] We use three measures of heat stress: daily maximum temperature, daily minimum temperature, and Heat Index. These metrics are most pronounced in the summer, which is the most responsive season in the Mediterranean hotspot [*Giorgi*, 2006]. We quantify changes in the 95th and 75th percentile daily maximum and minimum 2-meter air temperatures. Additionally, in order to capture the stress induced by the combined effects of high temperature and high humidity, we calculate apparent heat using the Heat Index [*Rothfusz*, 1990; *Steadman*, 1984], where:

$$\begin{aligned}\mathrm{HI} = & -42.379 + (2.04901523 \times \mathrm{T}) + (10.14333127 \times \mathrm{RH}) \\ & - (0.22475541 \times \mathrm{T} \times \mathrm{RH}) - \left(6.83783 \times 10^{-3} \times \mathrm{T}^2\right) \\ & - \left(5.481717 \times 10^{-2} \times \mathrm{RH}^2\right) \\ & + \left(1.22874 \times 10^{-3} \times \mathrm{T}^2 \times \mathrm{RH}\right) \\ & + \left(8.5282 \times 10^{-4} \times \mathrm{T} \times \mathrm{RH}^2\right) \\ & - \left(1.99 \times 10^{-6} \times \mathrm{T}^2 \times \mathrm{RH}^2\right)\end{aligned}$$

for

$$\mathrm{T} = 2\text{-meter air temperature}(^\circ\mathrm{F})$$

$$\mathrm{RH} = 2\text{-meter relative humidity(percentage)}.$$

The relationships are valid while temperature is above 26.667°C and relative humidity is above 40%. We screen for daily maximum Heat Index values that equal or exceed 105 (equivalent to 40.56°C), indicating "danger" or "extreme danger" for at-risk groups (http://www.nws.noaa.gov/om/heat/index.shtml).

3. Results

3.1. Performance of the Nested Modeling System

[9] In order to evaluate the ability of RegCM3 to simulate the extremes of daily maximum and minimum temperature, we have compared observed values at 10 locations throughout the model domain [*Klein-Tank et al.*, 2002] with the RegCM3-simulated values at the corresponding land grid points (Table 1). We evaluate the magnitude of the 75th and 95th percentile maximum and minimum daily 2-meter temperatures. The 75th percentile magnitude reflects the bottom of the warmest 3 months of the year, while the 95th percentile magnitude reflects the bottom of the warmest 2.5 weeks of the year. Because real-world boundary conditions (such as elevation and land cover) can vary within a single model grid-point and thus create physically-consistent discrepancies between the observed and simulated data, we consider grid-point comparisons to be a stringent evaluation of the RegCM3 performance.

[10] We find that RegCM3 is able to capture the 75th percentile magnitude within 2.8°C of observations at 7 of 10 locations for maximum daily temperature and at 8 of 10 locations for minimum daily temperature (Table 1). We also find that RegCM3 is able to capture the 95th percentile magnitude within 2.8°C of observations at 4 of 10 locations for maximum daily temperature and at 10 of 10 locations for minimum daily temperature. Overall agreement is strongest at Isparta, Paris, Prague and Zurich, with the RegCM3 value falling within 1°C of the observed value for 8 of the 16 fields and within 2.1°C for 16 of the 16 fields. Agreement is weakest for 95th percentile maximum temperature at locations with observed values of 29.9°C or greater (with the exception of Isparta).

3.2. Simulated Future Changes

[11] The magnitude of the 95th percentile daily maximum temperature increases by up to 8.5°C in the A2 scenario compared to the reference simulation (MED20A2 minus MED20RF) (Figure 1). The magnitude of the 75th percentile event increases by up to 7.5°C, with most areas showing greater warming of the 95th percentile magnitude than of the 75th percentile magnitude. Both maximum temperature metrics display a substantial deceleration effect (MED20B2 minus MED20A2), with intensification of 95th percentile maximum temperature magnitude reduced by up to 2.75°C in the B2 simulations compared with the A2 simulations, and intensification of 75th percentile maximum temperature magnitude reduced by up to 3°C (Figure 1).

[12] The magnitude of the 95th percentile daily minimum temperature increases by up to 7°C in the A2 scenario (Figure 1). Likewise, the magnitude of the 75th percentile magnitude increases by up to 6°C. As with the maximum temperature quantiles, increases in the 95th percentile magnitude are greater than increases in the 75th percentile magnitude. Further, there is also a substantial deceleration effect in the daily minimum temperature quantiles, with

Table 1. Comparisons of RegCM3-Simulated Extreme Temperatures With Observations at 10 Locations. Values in Parentheses Refer to the Change in the Number of Exceedences of the Respective Percentile Values in the MED20RF Simulation[a]

	T Max		T Min	
	95%	75%	95%	75%
		Paris		
Obs	26.9	20.9	16.7	12.8
RF	27.4	19.7	16.1	11.2
B2	33.7 (39)	23.7 (39)	18.9 (32)	13.6 (41)
A2	35.0 (49)	25.0 (50)	20.4 (49)	14.8 (59)
		Prague		
Obs	27.7	21.1	16.7	12.3
RF	28.4	19.6	15.9	10.5
B2	32.2 (19)	22.3 (28)	18.4 (27)	12.8 (32)
A2	34.1 (33)	24.2 (44)	19.7 (40)	14.0 (51)
		Zurich		
Obs	26.9	20.2	14.9	10.0
RF	25.6	18.1	15.0	10.6
B2	30.1 (29)	21.4 (36)	18.0 (35)	12.6 (39)
A2	31.9 (40)	22.8 (50)	19.2 (50)	13.8 (57)
		Bucharest		
Obs	31.3	25.8	23.6	18.7
RF	37.4	27.4	21.0	14.4
B2	41.1 (22)	30.7 (21)	24.3 (29)	17.2 (28)
A2	42.8 (35)	32.5 (35)	26.0 (45)	18.6 (41)
		Rome		
Obs	32.0	26.9	18.8	14.8
RF	37.2	28.5	21.2	15.6
B2	41.3 (30)	32.2 (26)	24.8 (38)	18.6 (40)
A2	42.8 (43)	34.0 (38)	26.2 (56)	20.1 (55)
		Valencia		
Obs	29.9	26.7	21.7	18.0
RF	35.5	29.5	20.8	16.9
B2	39.4 (37)	32.4 (31)	24.5 (54)	19.8 (38)
A2	40.2 (48)	33.6 (44)	25.6 (73)	21.2 (53)
		Athens		
Obs	32.9	28.3	23.8	19.8
RF	39.3	31.8	23.0	17.4
B2	42.8 (27)	34.8 (24)	26.7 (44)	20.5 (35)
A2	44.9 (48)	36.8 (39)	28.3 (63)	22.3 (48)
		Isparta		
Obs	31.8	26.5	15.9	11.3
RF	33.6	26.6	15.5	10.2
B2	38.1 (39)	30.1 (30)	19.4 (46)	13.4 (40)
A2	39.9 (62)	32.5 (44)	21.1 (66)	15.0 (53)
		Tel Aviv		
Obs	30.1	28.4	23.3	20.9
RF	38.0	32.7	20.5	17.7
B2	41.5 (35)	35.8 (52)	23.8 (77)	20.7 (59)
A2	42.7 (55)	36.9 (62)	24.7 (94)	21.7 (69)
		Algiers		
Obs	32.8	28.1	21.0	16.2
RF	40.7	32.2	23.8	18.5
B2	45.1 (23)	35.7 (34)	28.0 (40)	21.6 (39)
A2	46.4 (36)	37.1 (49)	29.3 (59)	23.0 (55)

[a]Calculated as in [*Diffenbaugh et al.*, 2005].

reductions in 95th percentile magnitude of up to 2.5°C and reductions in 75th percentile magnitude of up to 2°C.

[13] The direct response of heat stress to elevated GHG concentrations is enhanced by a positive surface moisture feedback. Root zone soil moisture decreases (MED20A2 minus MED20RF) over most of the domain, with peak decreases of up to 100 mm. Surface evapotranspiration also decreases over most land points, with peak negative changes of up to −2 mm/day over the Iberian Peninsula (Figure 2). Accordingly, surface sensible heat flux increases by up to 55 W/m^2, with the pattern of change closely following that of evapotranspiration (not shown). As with the temperature quantiles, the positive feedback associated with surface drying exhibits a deceleration effect, with decreases in evapotranspiration reduced by up to 1 mm/d in the B2 scenario (not shown).

[14] The combination of high near-surface air temperature and high near-surface humidity can produce apparent temperatures that pose risks for vulnerable groups. In the reference simulation, the number of days exhibiting dangerous or extremely dangerous Heat Index is generally greater in the southern and eastern Mediterranean than in the northern Mediterranean (Figure 3). Changes are positive throughout the domain in the A2 scenario, with peak changes of up to 65 d/yr (Figure 3). (B2 changes show a very similar pattern.) Coastal areas generally show greater increases than adjacent inland areas. In most areas, increases represent a substantial fractional change, including in the eastern and southern Mediterranean where baseline values are relatively high.

4. Discussion and Conclusions

[15] Intensification of heat stress in the Mediterranean hotspot is enhanced by preferential warming of the hot tail of the daily temperature distribution, with 95th percentile maximum and minimum temperatures showing greater increases than the respective 75th percentile temperatures (Figure 1). The response of the hottest temperatures is amplified by a surface moisture feedback, with the areas of largest increase in 95th percentile maximum and minimum daily temperatures (Figure 1) associated with peak decreases in surface evapotranspiration (Figure 2) and peak increases in sensible heat flux (not shown). These changes in evapotranspiration and sensible heat flux are in turn associated with decreases in root zone soil moisture and 2-meter relative humidity (Figure 2). This amplification of heat stress through surface drying is most pronounced in the areas that show the most pronounced preferential warming of the hot tail of the daily temperature distribution, including France, the northern Iberian Peninsula, and maritime areas of the northern and southwestern Mediterranean (Figures 1 and 2). Land-atmosphere coupling has been shown to be critical for the greenhouse response in Europe [*Seneviratne et al.*, 2006], and a similar GHG-induced surface moisture feedback has been identified in mid-latitudes of North America [*Diffenbaugh et al.*, 2005].

[16] The pattern of spatial heterogeneity in the Heat Index response is also regulated by fine-scale climate processes. For instance, the pattern of Heat Index response closely follows the pattern of topography in the region, with larger changes at lower elevations and smaller changes at higher elevations. This topographic control occurs largely because of the difference in baseline values at high and low elevations: even after GHG-induced warming, high elevation areas are still too cool to exceed the "dangerous" Heat Index threshold very often, whereas low elevation areas, which have higher baseline values (Figure 3), exceed the

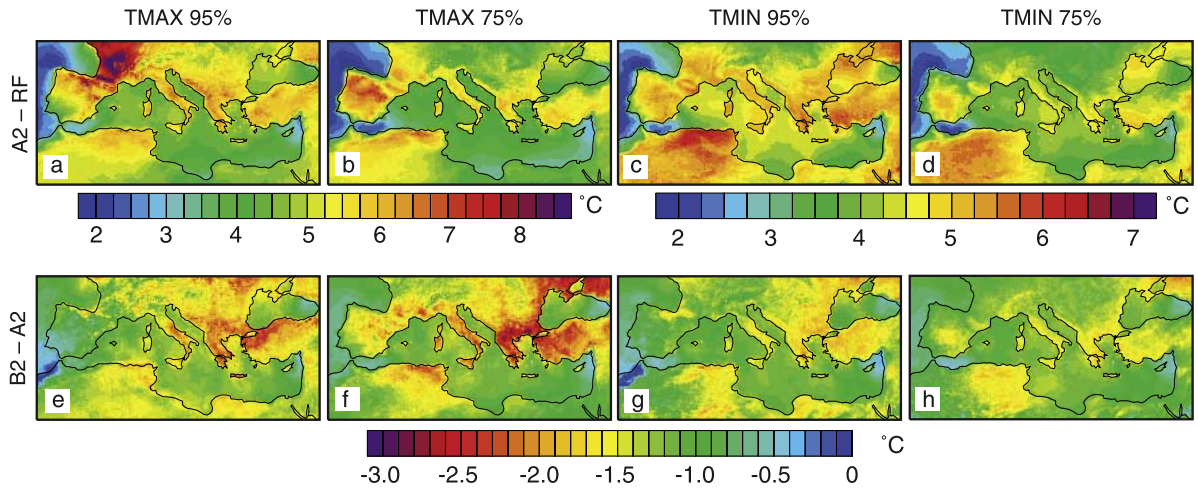

Figure 1. Change (MED20A2 minus MED20RF) in the magnitude of the (a) 95th percentile daily maximum 2-meter air temperature, (b) 75th percentile daily maximum 2-meter air temperature, (c) 95th percentile daily minimum 2-meter air temperature, and (d) 75th percentile daily minimum 2-meter air temperature (°C). Deceleration effect (MED20B2 minus MED20A2) for the magnitude of the (e) 95th percentile daily maximum 2-meter air temperature, (f) 75th percentile daily maximum 2-meter air temperature, (g) 95th percentile daily minimum 2-meter air temperature, and (h) 75th percentile daily minimum 2-meter air temperature (°C).

threshold much more frequently. Physiographic complexity thus partly contributes to the coastal amplification of the Heat Index response in the Mediterranean region, as many low elevation coastal areas are immediately adjacent to high elevation inland areas (Figure S1[1]). Further, the largest increases in dangerous and extremely dangerous conditions occur in areas where at present warm-season relative humidity is high at the coast and descends inland over relatively steep spatial gradients (Figure 2). In these areas, such gradients also contribute to coastal amplification of high Heat Index days, with relatively uniform increases in maximum temperatures having a larger effect on Heat Index in areas of high humidity (which occur near the coast) than in areas of low humidity (which occur away from the coast) (Figure 2). This humidity effect is particularly pronounced in the southern and eastern Mediterranean.

[17] Many areas of large extreme temperature response are associated with relatively large changes in the warm tail of the daily SST distribution (Figure 1). Although our experimental design captures the response of Mediterranean SSTs to large-scale climate changes induced by elevated GHG concentrations, the terrestrial heat stress response could be modified by atmosphere-ocean interactions occurring at finer spatial scales than those captured by the GCM. For instance, regional atmosphere-ocean coupling substantially reduces the Baltic Sea A2 SST response [*Kjellstrom et al.*, 2005]. Similar reductions in Mediterranean SST response could reduce the terrestrial heat stress response calculated here, particularly in coastal areas that are strongly influenced by adjacent ocean temperatures. Quantification of the role of fine-scale atmosphere-ocean feedbacks in shaping the heat stress response in the Mediterranean region would require application of a high-resolution coupled ocean-atmosphere modeling system.

[18] Of particular concern are potential changes in sea breezes in coastal areas of the Mediterranean. Sea breezes can moderate Mediterranean coastal climate through both onshore and offshore exchange of air masses [e.g., *Cros et al.*, 2004], with marine air masses penetrating inland on 10^2 km scales [*Cros et al.*, 2004]. Because the specific heat of continental material is less than the specific heat of ocean water, increases in GHG concentration could be expected to enhance land-sea thermal contrast and the intensity of coastal sea breezes. However, because the processes controlling subtle sea breeze dynamics are not captured at the resolutions employed here [e.g., *Case et al.*, 2002; *Colle et al.*, 2003], our calculated heat stress response ignores much of the potential influence of sea breeze changes. Quantification of such sea breeze effects would require application of higher resolution, non-hydrostatic modeling systems (as in the works by *Case et al.* [2002], *Colle et al.* [2003], and *Cros et al.* [2004]) over long model integrations (as in this study).

[19] The simulated heat stress response must be considered within the context of the identified model biases. These biases are relatively small for both 75th and 95th percentile daily minimum temperature magnitude (Table 1), indicating that RegCM3 is able to capture the processes important for high minimum temperatures in the Mediterranean region. This is likewise the case for high maximum temperatures in relatively cool locations. However, in locations with hotter maximum temperature extremes, RegCM3 does have a substantial warm bias at this resolution. This warm bias could indicate that the simulated future values are also too warm, or that feedbacks enhancing the simulated warming (such as the surface moisture feedback identified here) are muted by the fact that the model is beginning at an unrealistically warm baseline. Interestingly, the warm bias in extreme maximum temperature is substantially reduced in the lower resolution (50 km) simulation (Table S1). The fact that the response in the future scenarios is very close between

[1]Auxiliary material data sets are available at ftp://ftp.agu.org/apend/gl/2007gl030000. Other auxiliary material files are in the HTML.

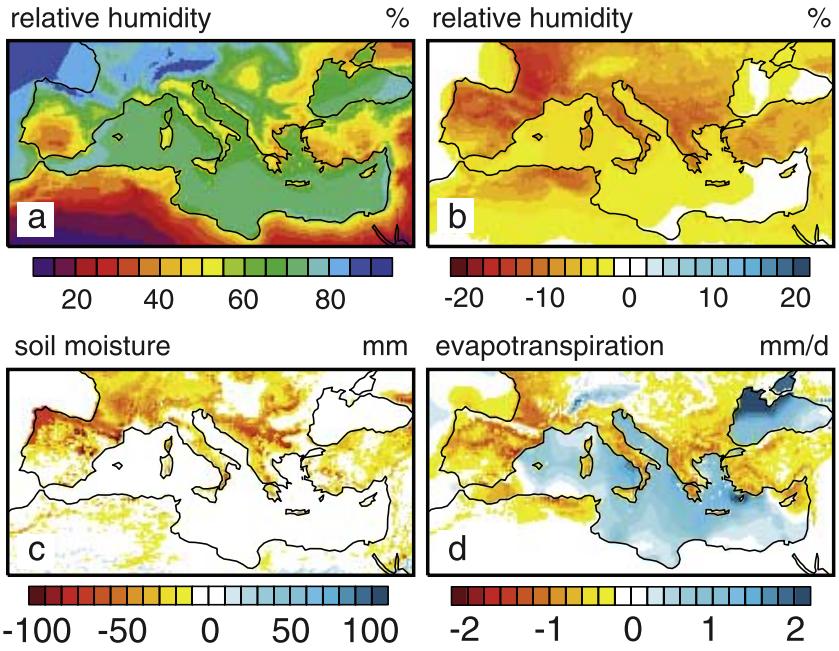

Figure 2. (a) JJA 2-meter relative humidity in the reference simulation (MED20RF) (percent). (b) Change (MED20A2 minus MED20RF) in JJA 2-meter relative humidity (percent). (c) Change (MED20A2 minus MED20RF) in JJA root zone soil moisture (millimeters). (d) Change (MED20A2 minus MED20RF) in JJA surface evapotranspiration (millimeters per day).

the two nested simulations (Table 1 and Table S1) suggests that perhaps the simulated changes are not heavily influenced by the model bias. (We note that the spatial coverage of daily humidity observations [*Klein-Tank et al.*, 2002] is insufficient to rigorously validate the Heat Index for the areas that show substantial response to elevated GHG concentrations. The fact that the model performance has not been validated for this metric should be considered when evaluating those results.)

[20] Should this simulated heat stress intensification actually occur, it could have substantial impact on human systems. At present, heat stress can exert substantial negative effects on human health [*Poumadere et al.*, 2005], energy supply and demand [*Smoyer-Tomic et al.*, 2003], hydrological resources [*Tereshchenko et al.*, 2002] and agricultural production [*Ferris et al.*, 1998; *White et al.*, 2006]. During the 2003 European heat-wave, peak excess deaths were closely associated with daily maximum and minimum temperatures that fell above the long-term 95th percentile values [*Grize et al.*, 2005; *Poumadere et al.*, 2005; *Schar et al.*, 2004] (Table 1). In our experiments, exceedences of the simulated 95th percentile reference temperatures at least triple in the A2 scenario (Table 1). Similarly, for most locations for which model output has been compared with observations, the A2-induced increases in 95th percentile temperature magnitude exceed the difference between the observed 95th and 75th percentile magnitudes. These substantial projected increases in the 95th percentile temperature magnitudes indicate that damaging heat stress could intensify in the coming decades should GHG concentrations continue to increase. However, we also find that emissions deceleration substantially reduces the response of heat stress to elevated GHG concentrations,

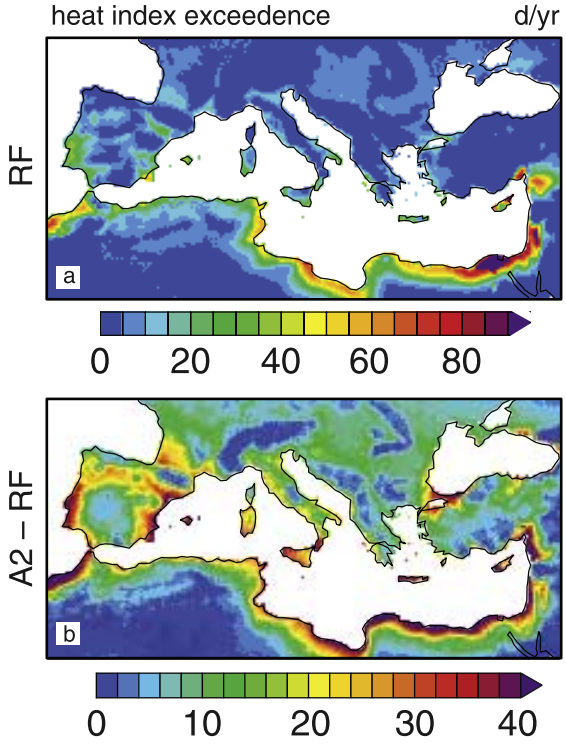

Figure 3. (a) The number of days in the reference simulation with dangerous or extremely dangerous Heat Index (MED20RF) (days per year). (b) The change in the number of days with dangerous or extremely dangerous Heat Index in the A2 emissions scenario (MED20A2 minus MED20RF) (days per year).

with emissions reductions in the B2 scenario reducing heat stress intensification by up to 50% for 95th percentile maximum and minimum temperature magnitude (Figure 1). Although this reduced response in the B2 scenario suggests that emissions deceleration could substantially mitigate the costs of climate change in the coming decades, increases in heat stress are still substantial in the B2 scenario, implying that further emission deceleration would be necessary to avoid costly heat stress intensification.

[21] **Acknowledgments.** We thank two anonymous reviewers for thorough and insightful comments, as well as A. Jain for helpful discussions regarding the emissions scenarios. This work was supported in part by the National Science Foundation (N.D.) and in part by the Italy-USA collaborative agreement on climate change research (X.G). This is PCCRC paper 0607.

References

Barnett, T. P., et al. (2005), Penetration of human-induced warming into the world's oceans, *Science*, *309*, 284–287, doi:10.1126/science.1112418.

Case, J. L., et al. (2002), Verification of high-resolution RAMS forecasts over east-central Florida during the 1999 and 2000 summer months, *Weather Forecasting*, *17*, 1133–1151.

Christensen, J. H., et al. (2002), PRUDENCE employs new methods to assess European climate change, *Eos Trans. AGU*, *83*, 147.

Colle, B. A., et al. (2003), Multiseason verification of the MM5. Part I: Comparison with the Eta model over the central and eastern United States and impact of MM5 resolution, *Weather Forecasting*, *18*, 431–457.

Cros, B., et al. (2004), The ESCOMPTE program: An overview, *Atmos. Res.*, *69*, 241–279.

Diffenbaugh, N. S., et al. (2005), Fine-scale processes regulate the response of extreme events to global climate change, *Proc. Natl. Acad. Sci. U. S. A.*, *102*, 15,774–15,778.

Ferris, R., et al. (1998), Effect of high temperature stress at anthesis on grain yield and biomass of field-grown crops of wheat, *Ann. Bot.*, *82*, 631–639.

Gao, X. J., et al. (2006), Projected changes in mean and extreme precipitation over the Mediterranean region from a high resolution double nested RCM simulation, *Geophys. Res. Lett.*, *33*, L03706, doi:10.1029/2005GL024954.

Giorgi, F. (2006), Climate change hot-spots, *Geophys. Res. Lett.*, *33*, L08707, doi:10.1029/2006GL025734.

Giorgi, F., et al. (2004a), Mean, interannual variability and trends in a regional climate change experiment over Europe. I. Present-day climate (1961–1990), *Clim. Dyn.*, *22*, 733–756.

Giorgi, F., et al. (2004b), Mean, interannual variability and trends in a regional climate change experiment over Europe. II: Climate change scenarios (2071–2100), *Clim. Dyn.*, *23*, 839–858.

Grize, L., et al. (2005), Heat wave 2003 and mortality in Switzerland, *Swiss Medical Weekly*, *135*, 200–205.

Intergovernmental Panel on Climate Change (2000), *Special Report on Emissions Scenarios*, 570 pp., Cambridge Univ. Press, Cambridge, U. K.

Intergovernmental Panel on Climate Change (2001), *Climate Change 2001: The Scientific Basis*, Cambridge Univ. Press, New York.

Johns, T. C., et al. (2003), Anthropogenic climate change for 1860 to 2100 simulated with the HadCM3 model under updated emissions scenarios, *Clim. Dyn.*, *20*, 583–612.

Kjellstrom, E., et al. (2005), Atmospheric response to different sea surface temperatures in the Baltic Sea: Coupled versus uncoupled regional climate model experiments, *Nord. Hydrol.*, *36*, 397–409.

Klein-Tank, A., et al. (2002), Daily dataset of 20th-century surface air temperature and precipitation series for the European Climate Assessment, *Int. J. Climatol.*, *22*, 1441–1453.

Luterbacher, J., et al. (2004), European seasonal and annual temperature variability, trends, and extremes since 1500, *Science*, *303*, 1499–1503.

Mears, C. A., and F. J. Wentz (2005), The effect of diurnal correction on satellite-derived lower tropospheric temperature, *Science*, *309*, 1548–1551.

Pal, J. S., et al. (2007), Regional climate modeling for the developing world: the ICTP RegCM3 and RegCNET, *Bull. Am. Meteorol. Soc.*, in press.

Poumadere, M., et al. (2005), The 2003 heat wave in France: Dangerous climate change here and now, *Risk Anal.*, *25*, 1483–1494.

Rayner, N. A., D. E. Parker, E. B. Horton, C. K. Folland, L. V. Alexander, D. P. Rowell, E. C. Kent, and A. Kaplan (2003), Global analyses of sea surface temperature, sea ice, and night marine air temperature since the late nineteenth century, *J. Geophys. Res.*, *108*(D14), 4407, doi:10.1029/2002JD002670.

Rothfusz, L. P. (1990), The heat index equation (or, more than you ever wanted to know about heat index), *Tech. Attachment, SR/SSD 90-23*, NWS S. Reg. Headquarters, Forth Worth, Tex.

Sanchez, E., et al. (2004), Future climate extreme events in the Mediterranean simulated by a regional climate model: A first approach, *Global Planet. Change*, *44*, 163–180.

Schar, C., et al. (2004), The role of increasing temperature variability in European summer heatwaves, *Nature*, *427*, 332–336.

Seneviratne, S. I., et al. (2006), Land-atmosphere coupling and climate change in Europe, *Nature*, *443*, 205–209.

Smoyer-Tomic, K. E., et al. (2003), Heat wave hazards: An overview of heat wave impacts in Canada, *Nat. Hazards*, *28*, 463–485.

Steadman, R. G. (1984), A universal scale of apparent temperature, *J. Clim. Appl. Meteorol.*, *23*, 1674–1687.

Tereshchenko, I., et al. (2002), El Nino 1997–98 and the hydrometeorological variability of Chapala, a shallow tropical lake in Mexico, *J. Hydrol.*, *264*, 133–146.

White, M. A., et al. (2006), Extreme heat reduces and shifts United States premium wine production in the 21st century, *Proc. Natl. Acad. Sci. U. S. A.*, *103*, 11,217–11,222.

N. S. Diffenbaugh, Purdue Climate Change Research Center and Department of Earth and Atmospheric Sciences, Purdue University, 550 Stadium Mall Drive, West Lafayette, IN 47907-2051, USA. (diffenbaugh@purdue.edu)

X. Gao, National Climate Center, Beijing 100081, China.

F. Giorgi, Abdus Salam International Centre for Theoretical Physics, Strada Costiera 11, I-34014 Trieste, Italy.

J. S. Pal, Frank R. Seaver College of Science and Engineering, Loyola Marymount University, 1 LMU Drive MS 8135, Los Angeles, CA 90045, USA.